# Time-Domain Observations of a Slow Precursor to the 1994 Romanche Transform Earthquake

Jeffrey J. McGuire,* Pierre F. Ihmlé, Thomas H. Jordan

Low-frequency spectral anomalies have indicated that some large earthquakes are preceded by extended episodes of smooth moment release, but the reality of these slow precursors has been debated because they have not been directly observed in the time domain. High-gain seismograms from the 14 March 1994 Romanche Transform event (moment magnitude $M_w$ 7.0) show a precursory ramp with a moment of $7 \times 10^{18}$ newton meters beginning about 100 seconds before the arrival of the high-frequency $P$ waves. This precursor was the initial phase of a slow component of slip that released nearly half of the total moment of the earthquake. Such behavior may be typical for large earthquakes on the oceanic ridge-transform system.

Since the early work of Kanamori and Cipar (*1*) on the great 1960 Chilean earthquake, episodes of slow, smooth moment release have been postulated to precede and initiate some large earthquakes. New techniques based on the use of low-frequency seismic spectra have recently been developed for the detection and analysis of slow precursors (*2*, *3*). Their application to a catalog of large events has revealed that slow precursors are rare in continents and convergence zones but appear to be common features of earthquakes on the oceanic ridge-transform system (*4*). For example, Ihmlé *et al.* (*3*) found that the great Macquarie Ridge earthquake of 23 May 1989, which had a moment magnitude ($M_w$) of 8.2, was preceded by a slow precursor with a moment release of about $3 \times 10^{20}$ newton meters (Nm), equivalent to a $M_w$ 7.6 event. However, no precursor was evident on high-gain broadband seismograms in the interval immediately before the arrival times of the high-frequency $P$ waves (*3*). This observation has led some to reject the slow-precursor hypothesis (*5*).

The detection of slow precursors as time-domain signals at teleseismic distances is difficult because the ambient level of seismic noise rises rapidly at frequencies below about 3 mHz (*6*). We report here the detection of such signals for the 14 March 1994 earthquake on the Romanche transform fault in the central Atlantic Ocean (Fig. 1) (*7*). This large earthquake ($M_w$ 7.0) comprised at least two ordinary ruptures: a small preshock (subevent A in Fig. 2) followed approximately 16 s later by the main shock (subevent B). At the lowest noise station, Tamanrasset, Algeria (TAM), a low-passed version of the $P$ wave showed a distinct ramp in front of the main shock (Fig. 2). The amplitude of the ramp exceeded the noise level for at least 100 s before the high-frequency (subevent A) arrival time, and there is some suggestion that its beginning may have preceded subevent A by as much as 300 s.

Although TAM showed the precursor most clearly, the signal was visible at all other stations at which the first swing of the low-passed, main-shock $P$ wave was greater than a factor of 3 above the noise level (upper part of Fig. 3). On each of the six records that satisfy this criterion, the main-shock $P$ wave was preceded by a ramp of the same polarity, and in all six records the ramp had a consistent relative slope and duration. Because the low-noise stations covered all four quadrants of the focal sphere and sampled epicentral distances ranging from 28° to 73°, these observations confirm that the ramp is a source signal with a radiation pattern similar to that of the main shock, rather than a propagation effect. Given the coherency of the six low-passed records, we stacked them to obtain a composite waveform (lower part of Fig. 3). When corrected for the group delay of the low-pass filter, the precursory ramp can be seen to occur at least 90 s before the subevent A arrival time. As illustrated in Fig. 3, a similar stack of another strike-slip earthquake yielded no such precursor (*8*).

The A and B subevents have an unusual space-time relation that also suggests precursory moment release. We picked the $P$-wave times of the two subevents on all records with clear arrivals (Fig. 4 and Table 1) (*9*), located them relative to the background seismicity (*10*), and aligned the seismicity with the Africa–South America plate boundary on a high-resolution map of the altimetric gravity field (Fig. 5) (*11*, *12*). We found that

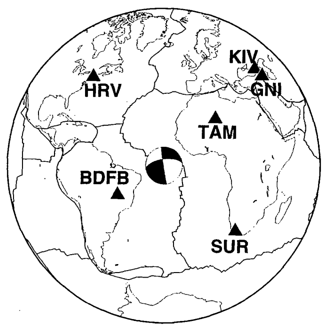


**Fig. 1.** Map showing the Harvard centroid moment tensor (CMT) location and mechanism of the 14 March 1994 Romanche Transform earthquake (*7*). Triangles show the locations of the six seismic stations used in the $P$-wave stack; these stations sample all four quadrants and lie away from nodes in the radiation pattern.

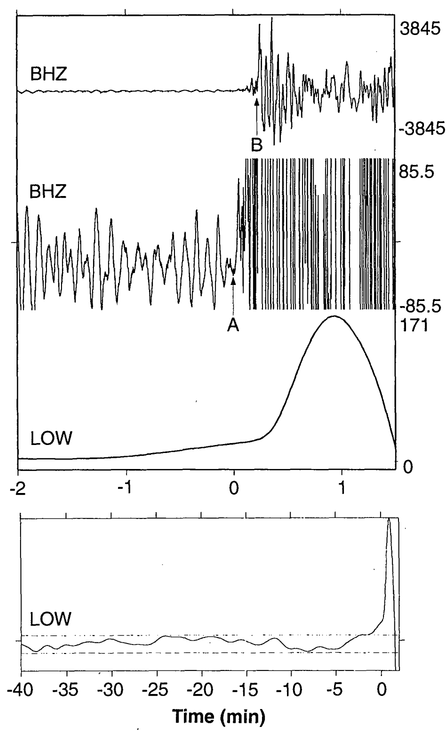


**Fig. 2.** Vertical-component records of the $P$ wave from the 1994 Romanche Transform earthquake at the high-performance seismic station TAM. The top panel shows the raw broadband trace at two magnifications (both labeled BHZ) and a detided, low-pass–filtered version of the same seismogram (labeled LOW), revealing the precursory ramp beginning at least 1 min before the high-frequency arrival time ($t$ = 0). The low-pass filter is a four-pole Butterworth with a 6-mHz corner. Vertical scales are digital units of the seismogram (counts). Arrows show the arrival-time picks for subevents A and B, with zero time set to be the high-frequency (subevent-A) arrival time. A comparison of the lower two traces in the top panel, which have the same magnification, shows that the amplitude of the high-frequency noise is substantially greater than that of the low-frequency precursor, masking the latter on the unfiltered record. The lower panel is the same low-passed record at a longer time scale, with dashed lines approximating the noise level. The two low-passed records have not been corrected for the group delay of the filter, which is 10 s.

J. J. McGuire and T. H. Jordan, Department of Earth, Atmospheric, and Planetary Sciences, Massachusetts Institute of Technology, Cambridge, MA 02139, USA.
P. F. Ihmlé, Institut de Physique du Globe, 4 Place Jussieu, Paris Cedex 75252, France.

*To whom correspondence should be addressed.

the two subevents were separated by 83 ± 15 km and 16.7 ± 1.0 s. Therefore, a model of the rupture initiating at subevent A and propagating directly to subevent B requires a rupture velocity of 5.0 ± 1.0 km/s, which exceeds the shear-wave speed in the upper oceanic lithosphere and thus the typical rupture velocity of shallow-focus earthquakes (*13, 14*). Moreover, the locations of subevents A and B lie along an azimuth of N37 ± 8°E, which is at a significant angle to the strikes of the inferred fault planes for both subevents (Fig. 5). These data suggest that the two events occurred on separate fault planes and were initiated by a common precursor.

The location of subevent A, the small preshock ($M_w \sim 6$), is consistent with its being on the primary active trace of the Romanche transform fault, but subevent B, the main shock, is located significantly north of this feature, in a valley with a trend nearly parallel to the transform fault (*15*). The directivity inferred from the azimuthal variation of the *P* waveforms indicates that the main shock propagated to the east. No aftershocks were teleseismically recorded, so we could not determine its rupture length, but standard scaling relations would imply that it was 50 to 70 km (*14*). This distance approximates the length of a seismic gap just south of the main shock, where the valley of the main fault trace is interrupted by a large bathymetric high (*15*).

**Table 1.** Differential times for subevents A and B together with the station azimuths and epicentral distances (*9*).

| Station | Azimuth (degrees) | Distance (degrees) | B − A time (s) |
|---|---|---|---|
| ECH | 25 | 56 | 12.4 |
| SSB | 25 | 53 | 11.3 |
| TAM | 48 | 37 | 10.8 |
| LBTB | 121 | 53 | 18.4 |
| BOSA | 125 | 54 | 14.5 |
| BDFB | 238 | 28 | 21.7 |
| LPAZ | 249 | 46 | 24.1 |
| SJG | 297 | 46 | 18.8 |
| ANMO | 305 | 85 | 14.5 |
| CCM | 310 | 73 | 16.8 |

It is not possible to locate the slow precursor relative to the main shock, but moment-tensor inversions exclude the possibility that the precursor occurred on a fault connecting subevents A and B (*12*). One scenario (among many) consistent with the available data is that smooth slip at depth in the normally aseismic region redistributed stress in the region and triggered seismicity in both the westernmost portion of the Romanche (subevent A) and the neighboring fault valley to the north of the seismic gap (subevent B).

We also investigated the 1994 Romanche Transform earthquake using the spectral synthesis and inversion methods applied in earlier studies of slow earthquakes (*2–4*). We estimated the amplitude (total-moment) spectrum $M_T(\omega)$ (Fig. 6A) and phase-delay (time-shift) spectrum $\Delta t(\omega)$ (Fig. 6B) of the source at 1-mHz intervals from 1 to 50 mHz, using a combination of body waves, surface waves, and free oscillations (*16, 17*). The different wave types yielded consistent results throughout their regions of overlap. The phase-delay spectrum is nearly constant across the entire frequency band, but the amplitude spectrum shows a sharp break at about 10 mHz. This pattern is similar to that observed for other slow earthquakes by Jordan (*2*) and Ihmlé and Jordan (*4*), which they interpreted as compound sources. According to this hypothesis, the amplitude break results from the superposition of an ordinary fast rupture, which dominates the spectrum at high frequencies, and a smooth transient of longer duration, which dominates at low frequencies. The lack of a corresponding break in the phase-delay spectrum requires that the centroid times of the two events be nearly equal, thus implying that the slower event begins first.

To quantify these statements, we performed a joint inversion of the spectra and the *P*-wave stack for the source time function (Fig. 6, C and D). The results show an event sequence that comprises a slow earthquake beginning 110 s before the high-frequency origin time ($t$ = 0) and continuing for about 250 s, a preshock initiating at 0 s, and a 29-s pulse of high moment release beginning at 16 s. This compound-event model fits the amplitude and phase-delay data across the entire frequency range, as well as the precursor observed in the waveform stack. We also inverted the spectral data alone, allowing no moment release at $t < 0$, but found that we could not simultaneously satisfy the large amplitudes and flat phase delays at low frequencies. Hence, the spectral data confirm the existence of the slow precursor seen in the *P*-wave stack.

The best fitting source time function has a total static (zero-frequency) moment of 5.4 × $10^{19}$ Nm. Comparing its amplitude spectrum to one from a source time function confined to the interval $0 \leq t \leq 40$ s (Fig. 6) indicates that the static moment released by the slow component is about 2.3 × $10^{19}$ Nm, or 43% of the total. About 0.7 × $10^{19}$ Nm (13%) is

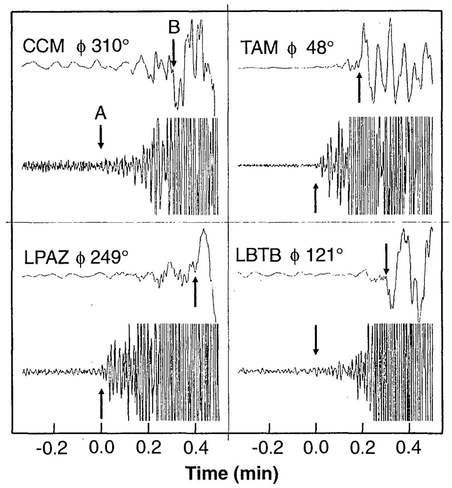


**Fig. 4.** Vertical-component *P* waves recorded at four stations, showing (arrows) the arrival-time picks for subevent A on high-pass–filtered seismograms (lower traces) and subevent B on unfiltered broadband seismograms (upper traces). Each trace runs from 20 s before to 30 s after the subevent-A arrival. The high-pass filter is a four-pole Butterworth with a 1-Hz corner; ϕ is the station azimuth. Stations to the northeast (for example, TAM) have smaller time differences between subevents A and B than stations to the southwest (for example, LPAZ), indicating that subevent B was located northeast of subevent A (*9*) (Table 1).

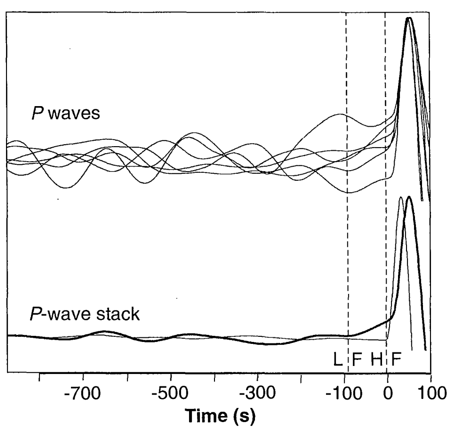


**Fig. 3.** Upper traces are vertical-component *P* waves for the 1994 Romanche Transform earthquake for the six low-noise stations shown in Fig. 1. These were the only stations for which the first swing of the main-shock *P* wave was greater than a factor of 3 above the noise level. All seismograms have been detided, low-pass–filtered (four-pole Butterworth with a corner at 6 mHz), corrected for the group delay of the filter, detrended, and corrected for radiation pattern (flipped in polarity if dilatational and normalized to a common amplitude). Lower traces are a stack of these six seismograms (heavy line) and a similar, six-station stack for the large ($M_w$ 7.0) Mendocino earthquake of 1 September 1994 (*8*) (light line). In both cases, zero time corresponds to the high-frequency arrival time (labeled HF). The Romanche Transform earthquake shows a precursory ramp beginning at or before −90 s (labeled LF), whereas the Mendocino earthquake does not. The delay in the arrival time of the high-amplitude *P* wave for the Romanche Transform earthquake corresponds approximately to the 16-s delay between subevent A, which is the first high-frequency arrival, and subevent B, which is the main shock.

released in the slow precursor.

Because slow earthquakes occur most frequently along oceanic transform faults, Ihmlé and Jordan (4) proposed that the intrinsic stratification of oceanic lithosphere may be responsible for their compound-event character. According to this hypothesis, fast ruptures in the shallow seismogenic zone are initiated by the loading due to slower episodes of slip in the subjacent (serpentinized?) upper mantle. The superposition of a fast event in the middle of a slow event, as seen in the source time function of Fig. 6D, is most easily accounted for by this depth relation.

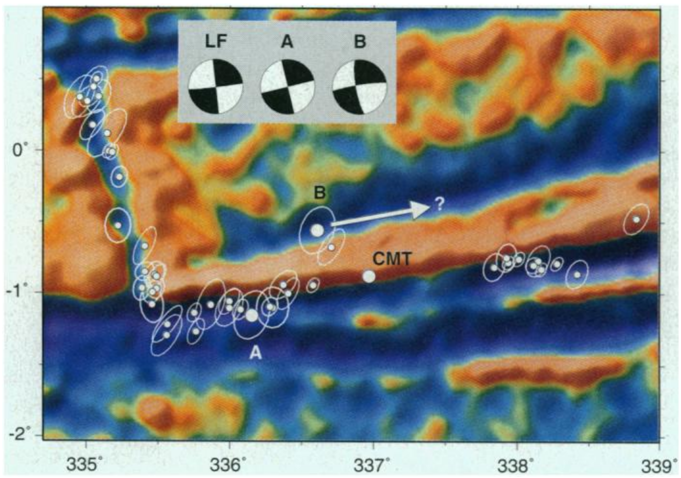


**Fig. 5.** Map of the western part of the Romanche Transform fault, showing the relocated earthquakes, plotted as points with 95% confidence ellipses (*10*), and the altimetric gravity field (*11*). Beachball insets are the low-frequency source mechanism (LF) and subevent mechanisms (A and B) for the 1994 Romanche Transform earthquake (*12*). Large dots represent the epicenters of subevents A and B and the Harvard CMT epicentroid, and the arrow emanating from B shows the direction and approximate length of the main rupture. The gravity anomalies range from −15 mgal (blue) to +15 mgal (red), and the relief is illuminated from the northwest.

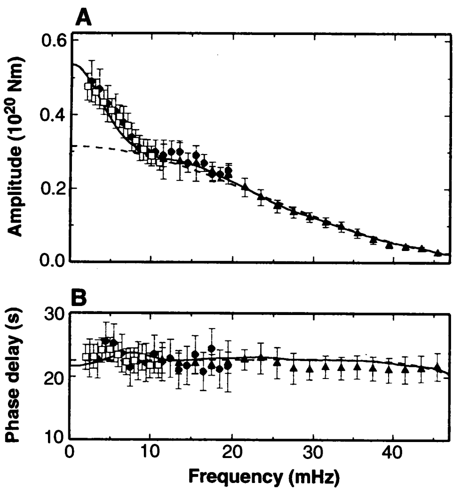


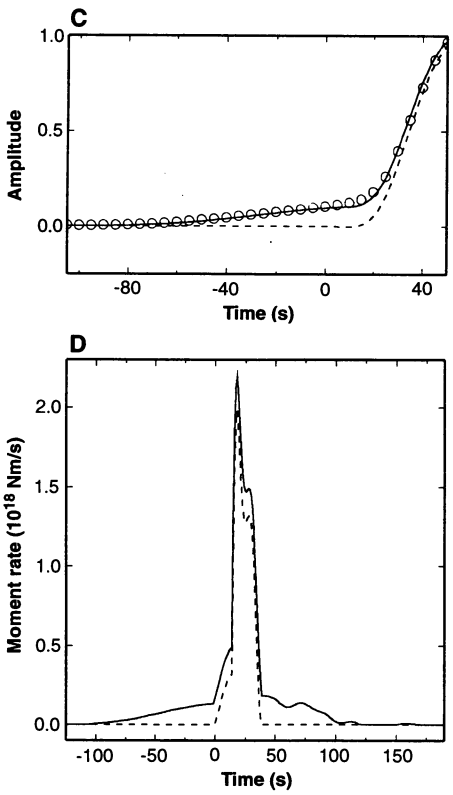


**Fig. 6.** (**A**) Amplitude and (**B**) phase-delay spectra for the 1994 Romanche Transform earthquake. Points are estimates with 1$\sigma$ error bars obtained from propagation-corrected spectra, averaged over a global network of 32 broadband stations (*16*); wave types used in the measurements are spheroidal free oscillations (solid circles), Rayleigh waves (open squares), and long-period body wave trains (solid triangles). Solid and dashed lines are the spectra obtained by Fourier-transforming the source time functions in (D). The phase-delay spectrum is referenced to the NEIC high-frequency origin time (*7*), which corresponds to the initiation of subevent A. (**C**) Comparison of the observed *P*-wave stack from Fig. 3 (open circles) with synthetic seismograms (solid and dashed lines) computed from the source time functions in (D). (**D**) the solid line is the source time function obtained by the joint inversion of the spectral-domain data in (A) and (B) and time-domain data in (C) (*17*). The dashed line is from the inversion of just the spectral data in the band from 10 to 50 mHz, where the time function was restricted to be zero for time less than 0 s and greater than 45 s.

The data presented here indicate that the slow precursor of the Romanche Transform earthquake grew for at least 100 s before it triggered a fast rupture, and the total moment released during the entire slow event was comparable to that of the main shock. This behavior appears to be common on oceanic transform faults (4), but it is in marked contrast to the nucleation phases observed for other earthquakes, which are small and accelerate quickly into inertia-dominated instabilities (*18*). The shape of the waveform stack and the absence of any observable high-frequency energy before subevent A indicate that the precursor's moment rate increased smoothly at a nearly linear rate, which implies that the product of the rupture and particle velocities during the slow phase of slippage must be at least two orders of magnitude smaller than that during the main shock (*19*). Hence, the designation "slow precursor" is truly warranted.

## REFERENCES AND NOTES


1. H. Kanamori and J. Cipar, *Phys. Earth Planet. Inter.* **9**, 128 (1974); see also I. L. Cifuentes and P. G. Silver, *J. Geophys. Res.* **94**, 643 (1989).
2. T. H. Jordan, *Geophys. Res. Lett.* **18**, 2019 (1991).
3. P. F. Ihmlé, P. Harabaglia, T. H. Jordan, *Science* **261**, 177 (1993).
4. P. F. Ihmlé and T. H. Jordan, *ibid.* **266**, 1547 (1994).
5. S. Kedar, S. Watada, and T. Tanimoto [*J. Geophys. Res.* **99**, 17893 (1994)] found significant amplitude and phase anomalies for certain low-frequency spheroidal modes that could be accounted for by a slow precursor to the Macquarie Ridge earthquake [see also J. Park, *Geophys. Res. Lett.* **17**, 1005 (1990)], but they rejected this possibility because no precursor was evident as time-domain signals preceding the *P* waves at high-gain seismic stations. Such signals would be below the noise level if the time function of the precursor were smooth and of sufficiently long duration (*3*).
6. D. Agnew and J. Berger, *J. Geophys. Res.* **83**, 5420 (1978); G. C. Beroza and T. H. Jordan, *ibid.* **95**, 2485 (1990).
7. The hypocenter location given by the National Earthquake Information Center (NEIC) is 94:03:14:04:30:07.7 UT (universal time), 1.08°S, 23.9°W, $h$ = 10 km; and the Harvard centroid location [A. M. Dziewonski, G. Ekström, M. P. Salganik, *Phys. Earth. Planet. Inter.* **86**, 253 (1994)] is 94:03:14:04:30:33.1 UT, 0.88°S, 23.0°W, focal depth = 15 km.
8. The Harvard centroid location [A. M. Dziewonski, G. Ekström, M. P. Salganik, *Phys. Earth. Planet. Inter.* **90**, 1 (1995)] for this right lateral $M_w$-7.0 event is 94:09:01:15:16:00.6 UT, 40.59°N, 125.78°W, focal depth = 15 km.
9. We picked 10 arrivals for subevent A and 11 for subevent B, obtaining at least two B − A differential travel times in each azimuthal quadrant (see Table 1).
10. We performed relocations by using the clustered-event algorithm of T. H. Jordan and K. A. Sverdrup [*Bull. Seismol. Soc. Am.* **71**, 1105 (1981)], which yields relative locations that are independent of common path anomalies. We relocated subevents A and B together with all events having 30 or more *P*-wave arrival times in the International Seismological Centre catalog from 1964 to 1987 and in the Preliminary Determination of Epicenters catalog from 1990 to 1995. All event depths were fixed at 10 km. The hypocentroid of this seismicity cluster has been shifted 12 km in the direction N30°E to align the seismicity with the plate boundaries observed in the gravity field. Although the arrival time data for the 2-year period 1988 through 1989 were unavailable, the PDE catalog shows no events in the aseismic region

between 22.3°W and 23.3°W.

11. D. Sandwell, *Eos* **76**, 149 (1995).
12. We determined the moment tensor in 1-mHz bands from 1 to 11 mHz, using the free-oscillation inversion method described by M. A. Riedesel, T. H. Jordan, A. F. Sheehan, and P. G. Silver [*Geophys. Res. Lett.* **13**, 609 (1986)]; no significant frequency dependence of the source mechanism was observed, which implies that the slow component of the 1994 Romanche Transform earthquake had a radiation pattern similar to that of the main shock. The mechanism labeled LF in Fig. 5 is the average across the frequency band 3 to 6 mHz. The source mechanisms of subevents A and B, also shown in Fig. 5, were determined by waveform analysis. They are similar but not identical; for example, their long-period *P*-wave polarities are reversed at Naña, Peru (NNA).
13. Although rupture velocities of shallow-focus earthquakes have been known to exceed the local shear-wave speed [R. Archuleta, *J. Geophys. Res.* **89**, 4559 (1984)], they are rare. Typical rupture velocities of shallow-focus earthquakes are less than 3.5 km/s (*14*).
14. C. H. Scholz, *The Mechanics of Earthquake Faulting* (Cambridge Univ. Press, Cambridge, 1990).
15. E. Bonatti, *et al.*, *J. Geophys. Res.* **99**, 21779 (1994); R. C. Searle, M. V. Thomas, E. J. W. Jones, *Mar. Geophys. Res.* **16**, 427 (1994). The morphology of the western portion of the Romanche Transform is extremely complex, exhibiting multiple paleotransform valleys that resulted from past changes in plate motions. The seismic gap on the main transform trace between 22.3°W and 23.3°W (Fig. 4) corresponds to a bathymetric high, which Searle *et al.* attributed to transpression caused by the northeastward bending of the fault trace at the western end of the gap. Locking of the main trace in this region could explain the offset of the B-subevent rupture to the north.
16. We obtained the spectral estimates in Fig. 6 using the procedures described in (*2–4*). We measured the spheroidal free oscillations from vertical-component seismograms in the band from 1 to 19 mHz, using the methods of P. G. Silver and T. H. Jordan [*Geophys. J. R. Astron. Soc.* **70**, 755 (1982)] and M. A. Riedesel and T. H. Jordan [*Bull. Seismol. Soc. Am.* **79**, 85 (1989)]. Measurements of first-orbit Rayleigh waves (1 to 10 mHz) and long-period body wave trains (10 to 50 mHz) were obtained from vertical-component seismograms by the methods of Ihmlé *et al.* (*3*). In all cases, synthetic seismograms were used to account for radiation-pattern and propagation effects. The synthetics were computed by mode summation from the Harvard CMT (*7*) and the degree-12 aspherical earth structure of W.-J. Su, R. L. Woodward, and A. M. Dziewonski [*J. Geophys. Res.* **99**, 6945 (1994)]. We also corrected fundamental modes above 7 mHz for smaller scale heterogeneity using the degree-36 phase-velocity maps of G. Ekström, J. Tromp, and E. W. Larson [*Eos* **74**, 438 (1993)].
17. We inverted the data using the quadratic programming algorithm of Ihmlé *et al.* (*3*), which minimizes a linear combination of a $\chi^2$ measure of data misfit and a quadratic form measuring the smoothness of the source time function, subject to the constraint that the source time function be nonnegative. The smoothing varied from high values before the subevent-A origin time ($110 \leq t < 0$ s), which ensured that the precursor did not generate significant high-frequency arrivals, to low values during the main-shock phase of the rupture ($16 \leq t < 45$ s), when the high-frequency amplitudes were largest; intermediate values of smoothing were assumed between the initiation of subevent A and the initiation of subevent B ($0 \leq t < 16$ s) and in the interval after the main shock ($40 \leq t < 200$ s).
18. W. L. Ellsworth and G. C. Beroza [*Science* **268**, 851 (1995)] have shown that the nucleation phases for typical earthquakes release about 0.5% of the total static moment $M_0$ and that the duration of nucleation varies as $M_0^{1/3}$. These scaling relations yield a nucleation phase with a moment of about $1.5 \times 10^{17}$ Nm and a duration of about 2 s for an earthquake the size of the 1994 Romanche Transform main shock.
19. For a rectangular fault of depth $D$ slipping at a constant particle velocity $\Delta\dot{u}$ and growing unilaterally at a rupture velocity $v_r$, the moment rate will increase at a rate $\ddot{M} = 2\,\mu\, D v_r \Delta\dot{u}$, where $\mu$ is the shear modulus. The observed moment acceleration for the slow precursor of the Romanche Transform earthquake is about $1.8 \times 10^{17}$ Nm/s$^2$. For $D = 10$ km and $\mu = 3 \times 10^{10}$ Pa, we obtain $v_r\,\Delta\dot{u} \approx 3$ m$^2$/s$^2$. Hence, if $v_r \approx 100$ m/s, $\Delta\dot{u} \approx 0.03$ m/s. In contrast, the observations for ordinary earthquakes, including the main shock of this event (Fig. 5), yield $v_r\,\Delta\dot{u} > 1000$ m$^2$/s$^2$.

20. We thank H. Webb for assistance with the gravity data and G. Ekström, J. Tromp, and E. Larson for the use of their unpublished phase-velocity maps. We are grateful to D. Wiens and an anonymous reviewer for helpful comments that improved the manuscript. Sponsored by NSF under grant EAR-9305081 and by NASA under grant NAG5-1905. P.F.I. was supported in part by the Swiss National Science Foundation.

18 June 1996; accepted 8 August 1996

# A Long Pollen Record from Lowland Amazonia: Forest and Cooling in Glacial Times

P. A. Colinvaux,* P. E. De Oliveira,† J. E. Moreno, M. C. Miller, M. B. Bush‡

**A continuous pollen history of more than 40,000 years was obtained from a lake in the lowland Amazon rain forest. Pollen spectra demonstrate that tropical rain forest occupied the region continuously and that savannas or grasslands were not present during the last glacial maximum. The data suggest that the western Amazon forest was not fragmented into refugia in glacial times and that the lowlands were not a source of dust. Glacial age forests were comparable to modern forests but also included species now restricted to higher elevations by temperature, suggesting a cooling of the order of 5° to 6°C.**

The Amazon lowlands in glacial times are widely thought to have been much drier than at present, even according to the "refuge hypothesis," so dry as to have prevented forest from occupying much of the basin (*1*), although this view has its critics (*2–6*). Many paleoecological data suggest cooling as a major climatic forcing in the Neotropics (*7–10*). We have tested the ice-age aridity and cooling hypotheses, using proxy data from Amazonian lake sediments (*11*).

Lake Pata lies below the 300-m contour on the Hill of the Six Lakes, a low inselberg of ancient plutonic rocks at 0°16′N, 66°41′W in the Amazon lowland of northwestern Brazil (*12*) (Fig. 1). The lowland vegetation of the region is dense tropical rain forest (DTRF) in a hot, humid climate (*13*).

All the lakes on the inselberg occupy small closed, steep-sided basins with flat or shelving bottoms under 7 to 15 m of water. The water level of one lake fell by about a meter in the 2 weeks of our visit, suggesting that the basins might not be completely sealed. The water is soft and acidic, which shows that these are not carbonate solution basins. A plausible hypothesis is that these are pseudo-karst lakes occupying basins formed by the solution of silica from ancient quarzitic rocks, perhaps dating from pre-Pleistocene times (*12*).

Lake Pata is about 300 m long and 7 m deep, and it occupies a large part of its forested catchment. We piston-cored the lake at its deepest point, reaching basement gravel under 7 m of lacustrine sediment. Seven accelerator mass spectrometer (AMS) radiocarbon dates, together with five β-decay dates, demonstrate that sedimentation has been continuous, roughly constant, and extremely slow, with an age of 30,000 years being reached in the first meter (*14*) (Table 1). The gross stratigraphy is simple: a surface unit (A) of soft blackish gyttja about 60 cm thick that grades over several centimeters into a yellower, firmer, and more granular unit (B) 20 cm thick, which in turn grades into a unit (C) of bluish black

P. A. Colinvaux, J. E. Moreno, M. B. Bush, Smithsonian Tropical Research Institute, Post Office Box 2072, Balboa, Panama (mail from the United States should be sent to the Smithsonian Tropical Research Institute, Unit 0948, APO AA 34002, USA).
P. E. De Oliveira, Field Museum, Roosevelt Road at Lake Shore Drive, Chicago, IL 60605, USA.
M. C. Miller, Department of Biology, University of Cincinnati, Cincinnati, OH 45221, USA.

*To whom correspondence should be addressed.
†Present address: Institute of Geosciencies-DPE, Universidade de Sao Paulo, Rua do Lago 562, 05508-900 Sao Paulo, SP Brazil.
‡Present address: Department of Botany, Duke University, Durham, NC 27708, USA.

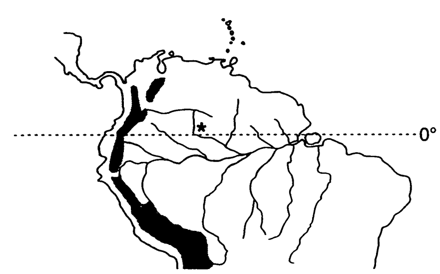


**Fig. 1.** Location map of the Hill of the Six Lakes (star) at 0°16′N, 66°41′W.